

# **In-situ synchrotron x-ray radiography on high temperature polymer electrolyte fuel cells**

Wiebke Maier<sup>a,\*</sup>, Tobias Arlt<sup>c</sup>, Christoph Wannek<sup>a</sup>, Ingo Manke<sup>c</sup>,  
Heinrich Riesemeier<sup>d</sup>, Philipp Krüger<sup>b</sup>, Joachim Scholta<sup>b</sup>, Werner Lehnert<sup>a</sup>,  
John Banhart<sup>c</sup>, Detlef Stolten<sup>a</sup>

<sup>a</sup> Institute of Energy Research, IEF-3: Fuel Cells, Forschungszentrum Jülich GmbH,  
52425 Jülich, Germany

<sup>b</sup> Zentrum für Sonnenenergie- und Wasserstoff-Forschung Baden-Württemberg,  
Helmholtzstr. 8, 89081 Ulm, Germany

<sup>c</sup> Helmholtz-Centre Berlin for Materials and Energy, Hahn-Meitner-Platz 1,  
14109 Berlin, Germany

<sup>d</sup> Bundesanstalt für Materialforschung und -prüfung, Richard-Willstätter-Str. 11,  
12489 Berlin, Germany

\* Corresponding author. Tel.: +49 2461 61 9073; fax: +49 2461 61 6695; E-mail  
address: [w.maier@fz-juelich.de](mailto:w.maier@fz-juelich.de).

# 1. Abstract

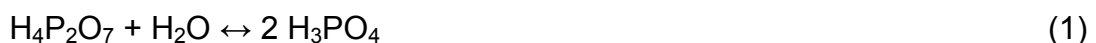
In contrast to classical low temperature polymer electrolyte fuel cells (PEFCs), the membrane conductivity in high temperature polymer electrolyte fuel cells (HT-PEFCs) (operating temperature  $\sim 160$  °C) is based on proton transport within phosphorus-oxygen acids at different levels of hydration, orthophosphoric acid ( $\text{H}_3\text{PO}_4$ ) being the simplest example. We present for the first time in-situ synchrotron x-ray radiography measurements applied to a HT-PEFC to gain insight into the local composition of the membrane electrode assembly (MEA) under dynamic operating conditions. Transmission changes during the radiographic measurements exhibit a clear influence of the formation of product water on the membrane composition.

## 1.1 *Keywords:*

HT-PEFC, synchrotron x-ray radiography, membrane electrode assembly (MEA), phosphoric acid

## 2. Introduction

Phosphoric acid doped polybenzimidazole as electrolyte for high temperature polymer electrolyte fuel cells (HT-PEFCs) with an operating temperature of about 160 °C exhibits good proton conductivity, low gas permeability and good mechanical stability at elevated temperatures [1]. To maximize the performance and lifetime of HT-PEFCs, it is necessary to design membrane electrode assemblies (MEAs) in which the distribution of the phosphoric acid between the membrane, the catalyst layers and the gas diffusion layers can be carefully adjusted [2]. The performance of a HT-PEFC with phosphoric acid doped polybenzimidazole as electrolyte is nearly independent of the way of acid introduction into the MEA but strongly depends on the amount inserted into it [3, 4, 5]. In order to achieve an optimum performance, high power densities and long lifetimes, it becomes necessary to provide excellent proton conductivity through the membrane. The composition of the membrane at 160 °C consists of a polybenzimidazole type membrane, in the present case poly(2,5-benzimidazole) (ABPBI), and phosphoric acid ( $\text{H}_3\text{PO}_4$ ) which forms an equilibrium with its dehydration products (mainly pyrophosphoric acid  $\text{H}_4\text{P}_2\text{O}_7$ ) [6, 7]. In the following we only will use the term phosphoric acid when talking about this equilibrium. The redistribution of the phosphoric acid and the hydration of the pyrophosphoric acid in the MEA is a fast process, accelerated by product water from the fuel cell operation. In case of a higher water formation it is also possible that the product water leads to a dissociation of the phosphoric acid:



These processes are believed to influence the local density of the different phosphoric acid type species in the MEA, the overall conductivity and viscosity of the electrolyte as well as the membrane composition and thus local physico-chemical properties of the HT-PEFC, such as proton conductivity and oxygen gas solubility. Up to now only averaging and ex-situ methods could be used to analyze the distribution of phosphoric acid. These methods include the measurement of the weight of the MEA components before doping, after doping and after cell operation tests [8], the determination of the phosphorous concentration in electrodes after cell operations test by acid-base-titration [9] and by optical emission spectroscopy with inductively coupled plasma [4]. For the investigation of dynamic effects inside the MEA, impedance spectroscopy can be performed [10]. Methods like cyclic voltammetry are able to reflect the actual working status of a MEA but the operating conditions have to be changed before a cyclic voltammogram can be recorded [9]. Therefore, highly temporal and spatial resolved in-situ measurements with synchrotron x-ray radiography were performed in order to gain insight into the local distribution of phosphoric acid in the MEA and the membrane without the need for intermitting the dynamic operating conditions. Until now synchrotron x-ray radiography was only applied to low temperature fuel cells for the investigation of the water content [11, 12] and for the investigation of the CO<sub>2</sub> evolution in direct methanol fuel cells [13].

### **3. Experimental**

#### *3.1 MEA preparation and single cell performance*

A commercially available gas diffusion layer (GDL) composed of a carbon fiber cloth with a microporous layer on one side (BASF Fuel Cell, E-TEK division) was coated with a dispersion of carbon-supported catalyst (20 % HP Pt on Vulcan XC-72, BASF

Fuel Cell), PTFE (Dyneon, 40% w/w in the final GDE) and dispersants by means of a doctor blade technique. The gas diffusion electrodes (GDE) were produced with a platinum loading of  $1.1 \text{ mg cm}^{-2}$ . After a drying step at room temperature the GDEs were doped with  $16.0 \text{ mg cm}^{-2}$  phosphoric acid and assembled with an undoped  $30 \text{ }\mu\text{m}$  thick Poly(2,5-benzimidazole) (ABPBI) membrane (FuMA-Tech) in a single test cell.

The cell was operated at  $160 \text{ }^\circ\text{C}$  and ambient pressure. For all experiments the mass flows of hydrogen and air for current densities equal to or greater than  $j = 140 \text{ mA cm}^{-2}$  (with a typical cell voltage of  $\sim 600 \text{ mV}$ ) have been adjusted to  $\lambda = 2/2$  (anode/cathode). For lower current densities the mass flows were fixed to a stoichiometry of those for  $j = 140 \text{ mA cm}^{-2}$ .

### 3.2 *Synchrotron x-ray radiography*

The radiographic measurements were performed at the synchrotron tomography station of the Helmholtz-Centre Berlin (HZB, BAMline, BESSY Germany). A monochromatic x-ray beam with an energy of  $30 \text{ keV}$  was used to ensure a sufficiently high transmission through the cell. An optical setup with a  $4008 \times 2672$  pixel CCD camera (PCO 4000 with a CdWO scintillator screen) was used to capture images with area sizes of up to  $8 \text{ mm} \times 8 \text{ mm}$  with pixel sizes between  $0.438 \text{ }\mu\text{m}$  and  $2.190 \text{ }\mu\text{m}$  and an optical spatial resolution of  $1\text{--}5 \text{ }\mu\text{m}$ . Typical exposure times per image were between  $4\text{--}6 \text{ s}$ , including a readout time of about  $1.5 \text{ s}$ .

In order to visualize changes in the MEA during different operating conditions, an energy was selected, that provides sufficient transmittance through the Pt-containing electrodes with their high attenuation coefficient – on the one hand – and sufficient sensitivity to phosphoric acid and water in the membrane and the GDLs – on the other hand. The attenuation coefficient  $\mu(E)$  of the materials contained in the MEA

were calculated for different energies. The results are shown in Tab. 1. We found  $E = 30$  keV is a good compromise between the feasibility to detect phosphoric acid in the membrane as well as in the high Pt-loaded electrodes.

A cell set-up with in-plane viewing direction was chosen for all experiments that allows to distinguish clearly between the GDLs, the electrodes and the membrane.

## 4. Results and Discussion

In Fig. 1 normalized images of the cross-section of a HT-PEFC at different operating conditions are displayed. All images, recorded during the measurements, were normalized with respect to an image of the cell after reaching a steady state (one hour after the break-in procedure) at open circuit voltage (OCV).

Fig. 1 a) shows radiographs of the HT-PEFC operated at 160 °C, ambient pressure and OCV. The radiograph at OCV is also normalized to itself. Therefore an image right at the beginning of the measurement at OCV was divided by the image of the cell after reaching the steady state. Due to this normalization and because of the high operation temperature, which causes little fluctuation within the cell, the MEA as well as the flow field edges of the cell can be seen in Fig. 1 a) and e). The membrane can be seen in the centre of the image. In the adjacent layers to the left and right side of the membrane the anode and cathode are visible, respectively, which are coated on the carbon cloth GDLs. An increase in membrane thickness depending on the current density was observed. The dry, undoped ABPBI membrane had a thickness of  $30 \pm 2$   $\mu\text{m}$ . After the assembly of the membrane with the doped electrodes and after the break-in procedure the thickness of membrane increased due to the phosphoric acid uptake from the electrodes into the dry membrane (see also [4]). At OCV a thickness of  $55 \pm 3$   $\mu\text{m}$  was measured as can be seen in Fig 1a). When switching

from OCV to a current density of  $j = 140 \text{ mA cm}^{-2}$ , a swelling of about  $10 \text{ }\mu\text{m}$  of the membrane could be observed (Fig. 1 b)). Hence, the membrane possesses a final thickness of  $65 \pm 3 \text{ }\mu\text{m}$  after an operation time of 15 min under load. A further increase in current density from  $j = 140 \text{ mA cm}^{-2}$  to  $j = 300 \text{ mA cm}^{-2}$  (Fig. 1 c)) and from  $j = 300 \text{ mA cm}^{-2}$  to  $j = 550 \text{ mA cm}^{-2}$  (Fig. 1 d)) does not lead to an additional swelling of the membrane, if at all, the resulting effects are too small to be visualized with this optical spatial resolution. This swelling process is reversible as can be seen from Fig. 1e. During one hour at OCV after the load-cycle changes the membrane exhibits the same thickness as before the load-cycle changes.

There are two possible explanations for the increase in membrane thickness: (i) the dilution/hydration of phosphoric acid in the membrane by product water and (ii) a transport of phosphoric acid from pores of the electrodes into the membrane. The two explanations as well as a combination of both would be a possible interpretation of the normalized radiographs of Fig. 1.

In order to determine which of the afore mentioned effects has the strongest impact on the increase in membrane thickness during load-cycle changes, the transmission signals (i.e. grey values) in the MEA were quantitatively analyzed. Therefore, different line scans with a horizontal width of about 1000 pixel have been evaluated for OCV,  $140 \text{ mA cm}^{-2}$ ,  $300 \text{ mA cm}^{-2}$  and  $550 \text{ mA cm}^{-2}$  (Fig. 2). Additionally, these scans are filtered by a Gaussian blur.

The measured radiographs display the actual transmission. Thus the grey values of these normalized radiographs directly correspond to a transmission change. A grey value  $> 1$  represents an increase in transmission in the actual radiograph compared to the reference image at OCV, while a grey value  $< 1$  refers to a decrease in

transmission. A grey value equal to one declares that there are no differences between the reference image at OCV and the actual operating condition.

The results given in Fig. 2 show that when switching the cell from OCV to a current density of  $j = 140 \text{ mA cm}^{-2}$  yields in an increased transmission in the membrane (M). This result can be explained by the formation of product water, that leads to a hydration of the dehydration products of the phosphoric acid and thus to a swelling of the membrane (conf. equation (1)). The attenuation coefficient of water is one order of magnitude smaller than that of phosphoric acid at the same x-ray energy. Thus, an increase of water in the membrane as well as a build-up of hydration products of phosphoric acid could lead to a smaller transmission due to a change in membrane/electrolyte composition. In a recent publication by Wippermann et al. [10] a similar mechanism has been proposed to describe changes in the impedance during load-cycle changes. Wippermann et al. operated a HT-PEFC at identical operating conditions.

But likewise the membrane thickness does not increase with a further rising of the current density as described before, the transmission within the membrane does not further increase with increasing current density. Hence, it is clearly visible that the biggest effect in membrane swelling as well as transmission change can be seen, when switching the cell from a currentless operating condition to one where current will be drawn and thus the formation of product water begins. The further increase of the drawn current does not lead to any further visible effects. This may be due to the fast hydration process at the beginning of the water production, because of the hygroscopic nature of phosphoric acid. A further increase in water production does not have such a great impact on the further hydration process in contrast to the beginning of the water formation.

The images in Fig. 2 show also another effect within the electrodes. In the membrane vicinity an increase in x-ray transmission can be seen. Faraway from the membrane, in the vicinity of the GDLs, the transmission within the anode A and the cathode C decreases when switching the operation mode from OCV to a current density of  $j = 140 \text{ mA cm}^{-2}$ . A possible reason for both effects could be the swelling of the membrane which leads to an increase in volume and thus to a shifting of the electrodes and the GDLs towards the flow field edges (image sections not shown here).

Another reason could be the hydration of phosphoric acid within the pores of the electrodes in the vicinity of the membrane which leads to an increase in transmission, too, because the dehydration products of phosphoric acid are hydrated by product water, that has a much smaller attenuation coefficient. At the same time in the vicinity of the GDLs an increased degree of filling of the pores of the electrodes with phosphoric acid would lead to a grey value smaller than one. The electrodes have not been completely saturated before, because a significant amount of the phosphoric acid diffused into the pores of the electrodes close to the membrane and into the membrane itself during the break-in procedure (see also [4]) thus a huge part of the pores at the GDL side remained nearly empty. Filling of these previously nearly empty pores would lead to an increase in absorption in the beam direction and thus to the found decrease in transmission. We expect that both effects contribute to the found transmission distribution in Fig. 2. However, up to now it is not clear which effect is the most important one and additional measurements are necessary.

## 5. Conclusion

In-situ synchrotron x-ray radiography was applied to a dynamically operated HT-PEFC. With this experimental technique it was possible to visualize changes of the electrolyte composition and distribution during load-cycle changes. Analyses of the x-ray transmission through the MEA give an estimation about the composition of the membrane at OCV and under load. It was found that the formation of product water directly influences the distribution of the transmission signal. The effect is reversible when switching back to OCV. A possibility to verify these experiments would be a combination of the radiographic measurements with in-situ performed impedance spectroscopy, which would directly provide information about the ohmic resistance at different operating conditions related to the membrane/electrolyte composition. Parallel to this impedance measurements over time at a constant frequency, which are currently being performed, will give information about the time-dependent impedance and thus give evidence if the cell is operated at steady state or not.

## 6. References

- [1] Y. L. Ma, J. S. Wainright, M. H. Litt, R. F. Savinell, *J. Electrochem. Soc.* 151 (2004) A8.
- [2] J. Mader, L. Xiao, T. J. Schmidt, B. C. Benicewicz, *Adv. Polym. Sci.* 216 (2008) 63.
- [3] C. Wannek, B. Kohnen, H. F. Oetjen, H. Lippert, J. Mergel, *Fuel Cells* 8 (2008) 87.
- [4] C. Wannek, I. Konradi, J. Mergel, W. Lehnert, *Int. J. Hydrogen Energy* 34 (2009) 9479.
- [5] C. Wannek, W. Lehnert, J. Mergel, *J. Power Sources* 192 (2009) 258.
- [6] R. F. Jameson, *J. Chem. Soc.* – (1959) 752.
- [7] D.-T. Chin, H. Chang, *J. Appl. Electrochem.* 19 (1989) 95.
- [8] Y. Oono, A. Sounai, M. Hori, *Journal of Power Sources* 189 (2009) 943.
- [9] K. Kwon, J. O. Park, D. Y. Yoo, J. S. Yi, *Electrochim. Acta* 54 (2009) 6570.
- [10] K. Wippermann, C. Wannek, H.-F. Oetjen, J. Mergel, W. Lehnert, *J. Power Sources* 195 (2010) 2806.
- [11] C. Hartnig, I. Manke, R. Kuhn, N. Kardjilov, J. Banhart, W. Lehnert, *Appl. Phys. Lett.* 92 (2008) 134106–1.
- [12] I. Manke, C. Hartnig, M. Grünerbel, W. Lehnert, N. Kardjilov, A. Haibel, A. Hilger, J. Banhart, H. Riesemeier, *Appl. Phys. Lett.* 90 (2007) 174105–1.
- [13] C. Hartnig, I. Manke, J. Schloesser, P. Krüger, R. Kuhn, H. Riesemeier, K. Wippermann, J. Banhart, *Electrochem. Commun.* 11 (2009) 1559.

## 7. Tables

Table 1.

Material	excitation energy <i>E</i> / keV	attenuation coefficient $\mu$ / cm <sup>-1</sup>
Pt	15	3299.0400
Pt	30	542.0750
H <sub>3</sub> PO <sub>4</sub>	30	1.0198
H <sub>2</sub> O	30	0.1572

# 8. Figures

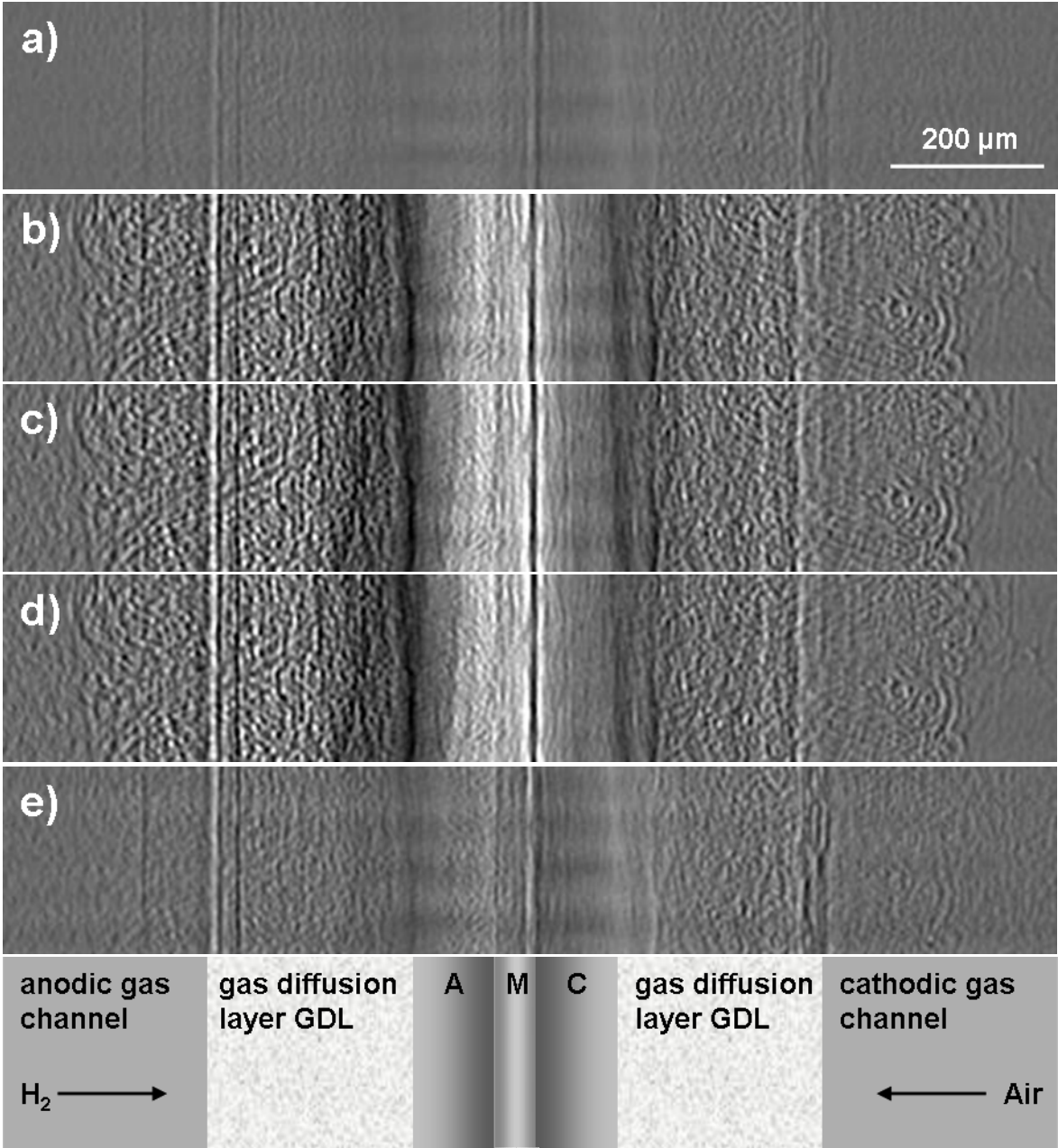


Figure 1.

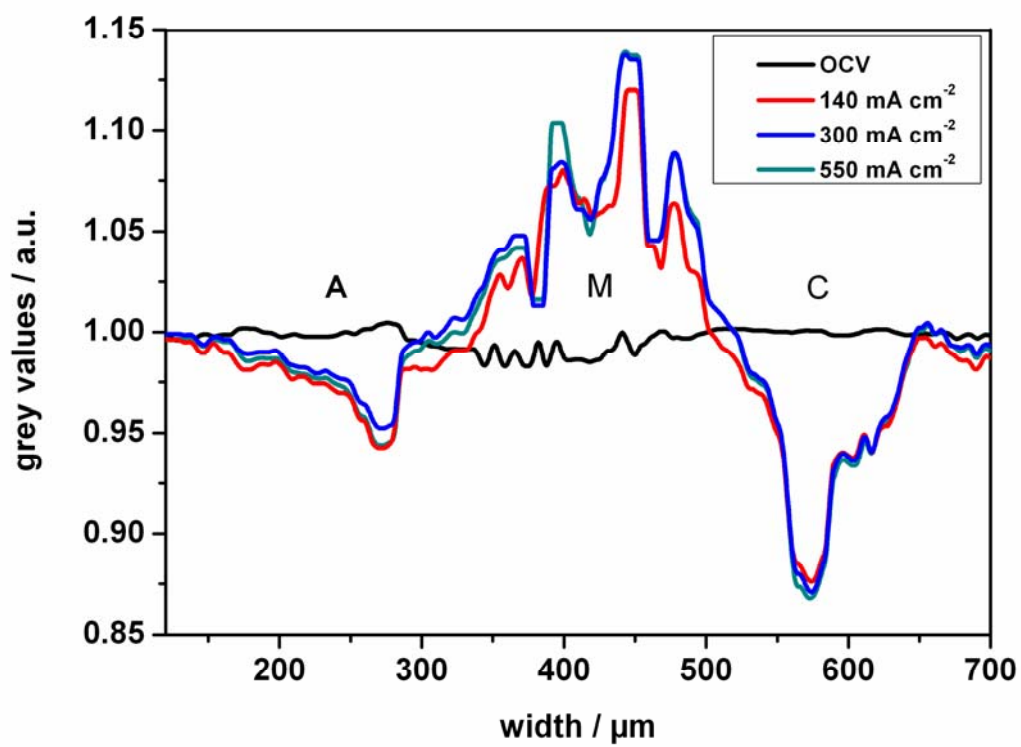


Figure 2.

## 9. Captions

### Table 1.

Attenuation coefficients for different materials and different excitation energies. (The data for the different materials should only represent an overview over the order of magnitude of the attenuation coefficients but do not give a statement about the appearance in an operated HT-PEFC.) (Data taken from the homepage “Centre of X-ray Optics” <http://www-cxro.lbl.gov/> 18.06.2010)

**Figure 1.** Normalized radiographs of the cross section of the MEA at different current density  $j$ : a)  $0 \text{ mA cm}^{-2}$  (OCV before), b)  $140 \text{ mA cm}^{-2}$ , c)  $300 \text{ mA cm}^{-2}$ , d)  $550 \text{ mA cm}^{-2}$  and e)  $0 \text{ mA cm}^{-2}$  (OCV after). (GDL, gas diffusion layer; A, anode; M, membrane; C, cathode)

**Figure 2.** Grey values within the MEA for different operating conditions at OCV,  $140 \text{ mA cm}^{-2}$ ,  $300 \text{ mA cm}^{-2}$  and  $550 \text{ mA cm}^{-2}$ . (A, anode; M, membrane; C, cathode)